Faraday Discussions

Cite this: *Faraday Discuss.*, 2017, **196**, 269

PAPER

Mesogenic gold complexes showing aggregation-induced enhancement of phosphorescence in both crystalline and liquid-crystalline phases†

Shigeyuki Yamada,‡ Yuki Rokusha, Ryo Kawano, Kaori Fujisawa§ and Osamu Tsutsumi*

Received 25th June 2016, Accepted 20th July 2016
DOI: 10.1039/c6fd00157b

Mesogenic Au complexes with a biphenyl core were synthesized as new AIEgens, and their thermodynamic and photophysical properties were discussed. Similar to Au complexes with a phenyl core which have been reported previously, the complexes with a short alkoxy chain formed dimers in the crystal form. However, the complexes with a long alkoxy chain formed two-dimensional layer structures through multiple intermolecular interactions in both the crystalline and liquid-crystalline (LC) phases. The present Au complexes showed a high thermochemical stability against thermal decomposition and a high thermodynamic stability of the LC phase. Moreover, these materials exhibited intensive phosphorescence with a large quantum yield (~66%) in the crystals. In the crystal and LC phase with a layer structure, the phosphorescence intensity was enhanced only on aggregation. Thus, these mesogenic Au complexes can be expected to be useful as phosphorescent AIEgens.

Introduction

Enormous efforts have been devoted to synthesise new luminescent organic molecules since they have been recognized as one of the most promising opto-electronic materials for organic light-emitting and electroluminescence devices.[1,2]

Department of Applied Chemistry, College of Life Sciences, Ritsumeikan University, 1-1-1 Nojihigashi, Kusatsu 525-8577, Japan. E-mail: tsutsumi@sk.ritsumei.ac.jp; Fax: +81-77-561-2659; Tel: +81-77-561-5966

† Electronic supplementary information (ESI) available: Full details of synthesis, characterisation of all the complexes, crystallographic data, XRD data of the Cry and Sme phases, DSC and TGA thermograms, and details of the photophysical characterisations including photoluminescence spectra of all the complexes. CCDC 1482940–1482945. For ESI and crystallographic data in CIF or other electronic format see DOI: 10.1039/c6fd00157b

‡ Present address: Faculty of Molecular Chemistry and Engineering, Kyoto Institute of Technology, Matsugasaki, Sakyo-ku, Kyoto 606-8585, Japan.

§ Present address: Department of Applied Chemistry, Faculty of Engineering, Aichi Institute of Technology, Yachigusa 1247, Yakusa, Toyota 470-0392, Japan.

Although a number of luminous organic molecules have been reported, most of them show strong photoluminescence only in a dilute solution; they are not emissive in the condensed phase due to aggregation-caused quenching.[3] However, in order to utilize luminescent molecules in practical applications, one of the most important characteristics is intensive photoluminescence in the condensed phase. Due to a growing demand for efficient luminescent materials in the condensed phase, new materials which luminesce in the condensed phase have been developed. Significant progress in this field has been made by Tang *et al.* since 2001. They first reported materials in which the luminescence was remarkably enhanced by the aggregation of molecules, called aggregation-induced emission (AIE).[4] Since this important discovery, new materials that possess AIE characteristics (AIEgens) have attracted huge interest as practical light-emitting materials.[5]

Among AIEgens, organometallic complexes containing d^{10} transition metals, *e.g.* Pt, Cu, Ag, and Au, have been paid much attention since they can show a fascinating luminescence behaviour in the condensed phase, triggered by metallophilic interactions.[6] In particular, Au(I) complexes have recently emerged as valuable AIEgens, since their luminescence behaviour can be varied by controlling the interatomic distance between Au atoms, namely through the strength of intermolecular Au/Au interactions.[7] Ito *et al.* conducted extensive studies on Au complexes and the developed Au complexes showed a change in the luminescence colour induced with a mechanical stimulus.[8]

We have also developed new Au complexes showing intensive photoluminescence in the condensed phase.[9] In particular, we have focused on Au complexes with liquid-crystalline (LC) properties to control their aggregated structures using external stimuli. Recently, we developed rod-shaped Au(I) complexes (**P*n***) which act as both a mesogen and a luminogen (Fig. 1a). The Au complexes, **P*n***, have a monocyclic core and showed photoluminescence not only in the crystalline (Cry) phase but also in the smectic (Sme) LC phase. Interestingly, we can reversibly control their luminescence colour from blue in the Cry phase to green in the Sme phase with a phase transition.[9b]

In order to apply such Au complexes possessing both photoluminescence and LC properties in practice, it is still necessary to enhance not only the photoluminescence efficiency in the condensed phase, but also the thermochemical stability of the molecules and the thermodynamic stability of the LC phase. To obtain Au complexes with such properties, we designed a suitable molecular

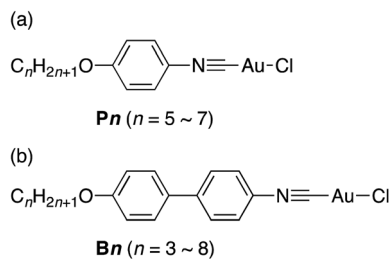

Fig. 1 Molecular structures of the gold complexes used in this study. The abbreviations of the molecules (P*n*, B*n*) are also indicated in the figure.

structure in which the Au complexes have (i) ligands with less steric bulkiness around the Au atom to facilitate the formation of Au/Au interactions, and (ii) core structures with a larger aspect ratio to enhance the stability of the LC phase. In this study, we synthesized new mesogenic Au complexes, **B*n***, with a bicyclic core structure and evaluated their thermal and photophysical properties to discuss the relationship between these properties and structures of the aggregates.

Experimental

Materials

Gold complexes **B*n*** (n = 3–8) were synthesized from the corresponding 4-alkoxy-4′-isocyanobiphenyl ligand and (tht)AuCl (tht = tetrahydrothiophene) according to the reported procedure with some modifications.[9b,10] Unless otherwise mentioned, all solvents and reagents were available from commercial suppliers and were used without further purification. Column chromatography was carried out with silica–gel (Wakosil® C-200, 64–210 μm) and thin-layer chromatography (TLC) analysis was performed on silica–gel TLC plates (Merck, Silica–gel 60 F_{254}). ^{1}H NMR spectra were recorded on a JEOL ECS-400 spectrometer at 400 MHz using the residual protons in the NMR solvent as an internal reference. Infrared (IR) spectra were observed using a KBr disk method with an FT/IR-610 (JASCO), and all spectra were reported in wavenumber (cm^{-1}). High-resolution mass spectra (HRMS) were taken with a JEOL JMS-700 spectrometer. Elemental analyses for C, H and N were conducted with a MICRO CORDER JM10 (J-SCIENCE).

Synthesis of (4-isocyano-4′-propoxy-1,1′-biphenyl)gold(I) chloride (B3). The corresponding isocyanide ligand (81 mg, 0.36 mmol) and (tht)AuCl (0.13 g, 0.42 mmol) were dissolved in dichloromethane and stirred at room temperature for 10 min. After removing the solvent, the crude product was washed with diethyl ether three times and purified using column chromatography on silica–gel (eluent: CH_2Cl_2). The product was further purified *via* recrystallization from a mixed solvent of ethanol and dichloromethane to afford (4-isocyano-4′-propoxy-1,1′-biphenyl)gold(I) chloride (**B3**) in 71% yield (0.12 g, 0.25 mmol) as pale yellow plate crystals. Mp 218 °C. ^{1}H NMR ($CDCl_3$): δ 7.67 (d, J = 8.6 Hz, 2H, 3′,5′-*H* in biphenyl), 7.56 (d, J = 8.6 Hz, 2H, 2′,6′-*H* in biphenyl), 7.52 (d, J = 8.6 Hz, 2H, 2,6-*H* in biphenyl), 7.00 (d, J = 8.6 Hz, 2H, 3,5-*H* in biphenyl), 3.98 (t, J = 6.7 Hz, 2H, OCH_2), 1.84 (qt, J = 7.1, 6.7 Hz, 2H, OCH_2CH_2), 1.06 (t, J = 7.1 Hz, 3H, CH_3). IR (KBr): ν 3043, 2967, 2880, 2224, 1493, 1294, 1176, 1011, 970 cm^{-1}. HRMS (FAB) m/z $[M]^+$ calcd for $C_{16}H_{15}AuClNO$ 469.0508; found 469.0524. Anal. calcd for $C_{16}H_{15}AuClNO$: C, 40.91; H, 3.22; N, 2.98. Found: C, 40.60; H, 2.95; N, 2.96.

Synthesis of B*n* (n = 4–8). According to the above procedure, **B*n*** (n = 4–8) were obtained from the corresponding isocyanide in 40–84% yields.

*(4-Butoxy-4′-isocyano-1,1′-biphenyl)gold(I) chloride (**B4**).* Yield: 83% (0.14 g, 0.29 mmol). Mp 170 °C. ^{1}H NMR ($CDCl_3$): δ 7.67 (d, J = 8.6 Hz, 2H, 3,5-*H* in biphenyl), 7.56 (d, J = 8.6 Hz, 2H, 2,6-*H* in biphenyl), 7.52 (d, J = 8.6 Hz, 2H, 2′,6′-*H* in biphenyl), 7.00 (d, J = 8.6 Hz, 2H, 3′,5′-*H* in biphenyl), 4.02 (t, J = 6.3 Hz, 2H, OCH_2), 1.80 (tt, J = 7.5, 6.3 Hz, 2H, OCH_2CH_2), 1.51 (tq, J = 7.5, 7.1 Hz, 2H, $OCH_2CH_2CH_2$), 0.99 (t, J = 7.1 Hz, 3H, CH_3). IR (KBr): ν 3042, 2957, 2870, 2220, 1492, 1246, 1067, 910 cm^{-1}. HRMS (FAB) m/z $[M]^+$ calcd for $C_{17}H_{17}AuClNO$ 483.0664; found 483.0679. Anal. calcd for $C_{17}H_{17}AuClNO$: C, 42.21; H, 3.54; N, 2.90. Found: C, 41.82; H, 3.24; N, 2.85.

*(4-Isocyano-4′-pentyloxy-1,1′-biphenyl)gold(I) chloride (**B5**).* Yield: 83% (0.14 g, 0.28 mmol). Mp 141 °C. ^{1}H NMR ($CDCl_3$): δ 7.67 (d, J = 8.6 Hz, 2H, 3′,5′-*H* in biphenyl), 7.56 (d, J = 8.6 Hz, 2H, 2′,6′-*H* in biphenyl), 7.52 (d, J = 8.6 Hz, 2H, 2,6-*H* in biphenyl), 7.00 (d, J = 8.6 Hz, 2H, 3,5-*H* in biphenyl), 4.01 (t, J = 6.7 Hz, 2H, OCH_2), 1.82 (tt, J = 7.1, 6.7 Hz, 2H, OCH_2CH_2), 1.51–1.34 (m, 4H, $CH_2CH_2CH_3$), 0.94 (t, J = 7.5 Hz, 3H, CH_3). IR (KBr): ν 3035, 2956, 2220, 1607, 1474, 1255, 1031, 891 cm^{-1}. HRMS (FAB) m/z $[M]^+$ calcd for $C_{18}H_{19}AuClNO$ 497.0821; found 497.0817. Anal. calcd for $C_{18}H_{19}AuClNO$: C, 43.43; H, 3.85; N, 2.81. Found: C, 43.14; H, 3.36; N, 2.82.

*(4-Hexyloxy-4′-isocyano-1,1′-biphenyl)gold(I) chloride (**B6**).* Yield: 84% (0.40 g, 0.79 mmol). Mp 141 °C. ^{1}H NMR ($CDCl_3$): δ 7.67 (d, J = 8.6 Hz, 2H, 3,5-*H* in biphenyl), 7.56 (d, J = 8.6 Hz, 2H, 2,6-*H* in biphenyl), 7.52 (d, J = 8.6 Hz, 2H, 2′,6′-*H* in biphenyl), 7.00 (d, J = 8.6 Hz, 2H, 3′,5′-*H* in biphenyl), 4.01 (t, J = 6.3 Hz, 2H, OCH_2), 1.81 (tt, J = 7.5, 6.3 Hz, 2H, OCH_2CH_2), 1.54–1.42 (m, 2H, $OCH_2CH_2CH_2$), 1.40–1.31 (m, 4H, $O(CH_2)_3CH_2CH_2$), 0.91 (t, J = 7.1 Hz, 3H, CH_3). IR (KBr): ν 3035, 2954, 2220, 1494, 1222, 1128, 1034, 994 cm^{-1}. HRMS (FAB) m/z $[M]^+$ calcd for $C_{19}H_{21}AuClNO$, 511.0977; found, 511.0995. Anal. calcd for $C_{19}H_{21}AuClNO$: C, 44.59, H: 4.14, N: 2.74. Found, C, 44.25; H, 3.93; N, 2.78.

*(4-Heptyloxy-4′-isocyano-1,1′-biphenyl)gold(I) chloride (**B7**).* Yield: 40% (0.22 g, 0.42 mmol). Mp 130 °C. ^{1}H NMR ($CDCl_3$): δ 7.67 (d, J = 8.6 Hz, 2H, 3,5-*H* in biphenyl), 7.56 (d, J = 8.6 Hz, 2H, 2,6-*H* in biphenyl), 7.52 (d, J = 8.6 Hz, 2H, 2′,6′-*H* in biphenyl), 7.01 (d, J = 8.6 Hz, 2H, 3′,5′-*H* in biphenyl), 4.01 (t, J = 6.7 Hz, 2H, OCH_2), 1.81 (tt, J = 7.1, 6.7 Hz, 2H, OCH_2CH_2), 1.51–1.27 (m, 8H, $OCH_2CH_2(CH_2)_4$), 0.90 (t, J = 6.7 Hz, 3H, CH_3). IR (KBr): ν 3034, 2953, 2220, 1495, 1254, 1127, 1040, 989 cm^{-1}. HRMS (FAB) m/z $[M]^+$ calcd for $C_{20}H_{23}AuClNO$, 525.1134; found, 525.1126. Anal. calcd for $C_{20}H_{23}AuClNO$: C, 45.68, H, 4.41; N, 2.66. Found, C, 45.35; H, 3.93; N, 2.68.

*(4-Isocyano-4′-octyloxy-1,1′-biphenyl)gold(I) chloride (**B8**).* Yield: 83% (0.14 g, 0.26 mmol). Mp 133 °C. ^{1}H NMR ($CDCl_3$): δ 7.67 (d, J = 8.6 Hz, 2H, 3′,5′-*H* in biphenyl), 7.56 (d, J = 8.6 Hz, 2H, 2′,6′-*H* in biphenyl), 7.52 (d, J = 8.6 Hz, 2H, 2,6-*H* in biphenyl), 7.00 (d, J = 8.6 Hz, 2H, 3,5-*H* in biphenyl), 4.01 (t, J = 6.3 Hz, 2H, OCH_2), 1.81 (tt, J = 7.1, 6.3 Hz, 2H, OCH_2CH_2), 1.52–1.43 (m, 2H, $OCH_2CH_2CH_2$), 1.41–1.24 (m, 8H, $O(CH_2)_3(CH_2)_4$), 0.89 (t, J = 7.1 Hz, 3H, CH_3). IR (KBr): ν 3035, 2955, 2221, 1496, 1224, 1128, 1034, 851 cm^{-1}. HRMS (FAB) m/z $[M]^+$ calcd for $C_{21}H_{25}AuClNO$, 539.1290; found, 539.1305. Anal. calcd for $C_{21}H_{25}AuClNO$: C, 46.72; H, 4.67; N, 2.59. Found, C, 46.30; H, 4.30; N, 2.51.

Phase transition properties

LC behaviours were observed using polarizing optical microscopy (POM) with an Olympus BX51 equipped with a hot stage (Instec HCS302 hot stage and mK1000 controller). To assess the thermochemical stability, thermogravimetric analysis (TGA) was carried out using a DTG-60AH (Shimadzu) at a heating rate of 5.0 °C min^{-1}. The thermodynamic parameters were determined using differential scanning calorimetry (DSC) (SII X-DSC7000) at a scanning rate of 5.0 °C min^{-1}. At least three scans were performed to check the reproducibility. The interlayer spacing of the Sme A phase was estimated with X-ray diffractometry (XRD) using an Ultima IV XRD-DSC IIx (Rigaku) with a D/tex-Ultra detector for the small angle region and a scintillation counter for the wide angle region. The temperature was

controlled with a built-in DSC unit (Rigaku, ThermoPlus2, DSC8230) at a scanning rate of 10 °C min^{-1}.

Photophysical properties

UV-visible absorption and steady-state photoluminescence spectra were recorded on a JASCO V-550 absorption spectrometer and a Hitachi F-7000 fluorescence spectrometer with R928 photomultiplier (Hamamatsu) as detector, respectively. The same crystals prepared for the single-crystal X-ray structure analysis were used for measurements in the Cry and LC states. The crystals were placed between a pair of quartz plates and set on a homemade heating stage to record the spectra at a controlled temperature. Photoluminescence quantum yields were determined using a calibrated integrating sphere (Hitachi). Photoluminescence lifetimes were measured with a Nd:YAG laser (Continuum, Minilite II: $\lambda = 355$ nm; pulse width = 4 ns, fwhm; repetition rate = 10 Hz) and decay profiles were recorded with a streak camera (Hamamatsu, C7700).

X-ray crystallography

Single crystals were prepared *via* slow evaporation of a mixed solvent system (ethanol/CH_2Cl_2). The crystal obtained was mounted on a glass fibre. The omega scanning technique was used to collect the reflection data using a Bruker D8 goniometer with monochromatized MoKα radiation ($\lambda = 0.71075$ Å). In order to estimate the actual crystal structure of the materials, the measurements were performed at ambient temperature (296 K). The initial structure of the unit cell was determined using a direct method with APEX2. The structural model was refined using a full-matrix least-square method with SHELXL-2014/6 (Sheldrick, 2014). All calculations were performed using SHELXL software. The crystal data of the Au complexes disclosed in this paper are summarized in the ESI and are indexed and included in the Cambridge Crystallographic Centre (CCDC) database with the following reference numbers: CCDC 1482940–1482945 for **B3–B8**.†

Results and discussion

Crystal structures of Au complexes

The Au complexes, **B*n*** ($n = 3$–8), were synthesized according to a previous report with some modifications.[11] 4-Alkoxy-4′-isocyanobiphenyl ligands were prepared from commercially available 4-nitro-4′-hydroxybiphenyl in four steps. The ligands were then treated with (tht)AuCl to yield the desired complexes as crystals after dual purification with silica–gel column chromatography and further recrystallization. The synthesis and characterization of the complexes **B*n*** ($n = 4, 6, 8$) have already been reported by Benouazzane *et al.*,[10] and the same spectral data were obtained here for these materials. The new complexes **B*n*** ($n = 3, 5, 7$) were fully characterized using ^{1}H NMR, IR, HRMS, elemental analysis and X-ray crystallographic analysis.

All complexes successfully gave single crystals from a slow evaporation technique using a mixed solvent system (ethanol/dichloromethane). The crystal structures of **B3**, **B5** and **B7** are shown in Fig. 2 as representative examples. The other materials showed almost the same crystal structures, as can be seen in the ESI (Fig. S2†). In addition, different crystal packing structures were observed

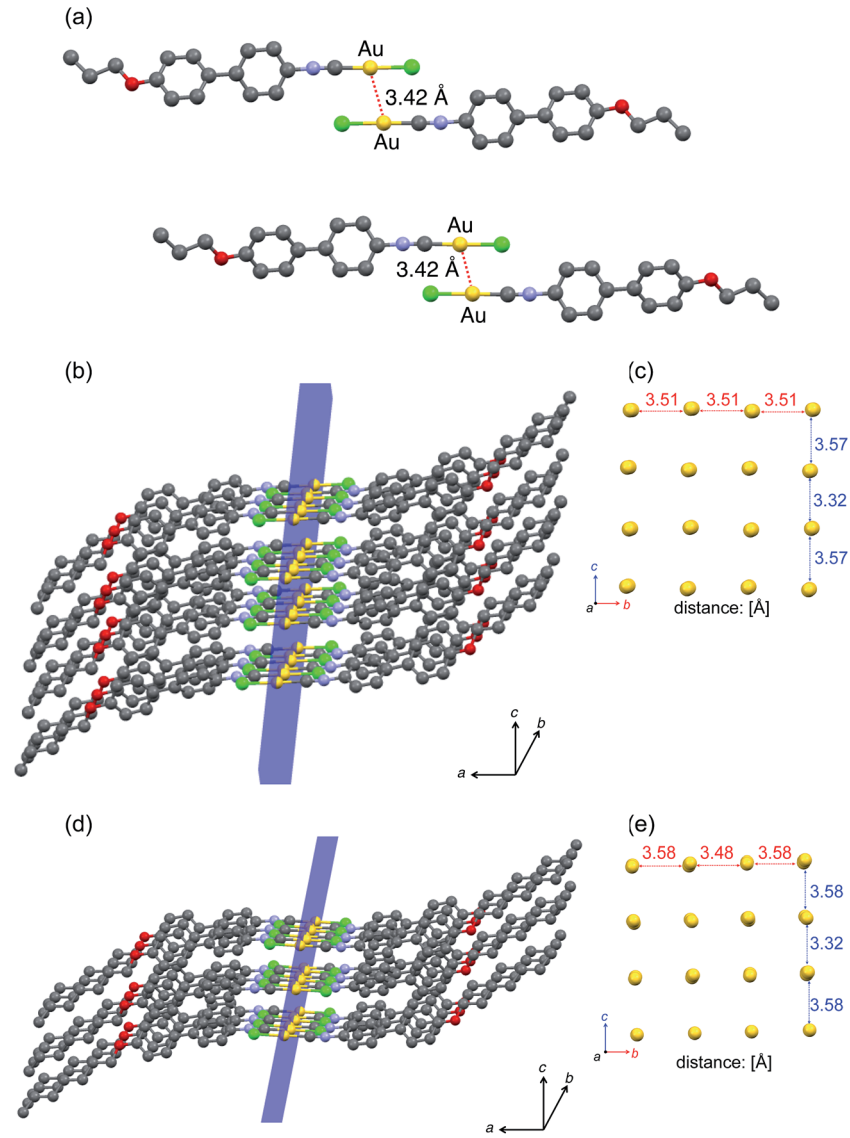

Fig. 2 Crystal structures of selected Au complexes: (a), **B3**; (b), **B5**; (d), **B7**. Hydrogen atoms are omitted for clarity. Colour legend: grey, carbon; red, oxygen; blue, nitrogen; green, chlorine; yellow, gold. Blue planes indicate a two-dimensional plane, where Au atoms are arranged with Au/Au interactions. (c) and (e) show arrangements of the Au atoms viewed along the *a*-axis.

between **B3–B4** and **B5–B8**. The former have a shorter alkoxy side chain that formed a dimer in the crystal, whereas the latter have relatively longer alkoxy moieties, forming well-ordered two-dimensional layer structures. The **B3** molecule was arranged with an anti-parallel orientation in the crystal, and the interatomic Au···Au distance was estimated to be 3.42 Å (Fig. 2a), which is below the sum of the van der Waals radius of two Au atoms (3.7 Å).[11] This suggests that **B3**

formed a dimer with a Au/Au intermolecular interaction, also known as an aurophilic interaction.[7] In contrast, in the crystals of **B5–B8**, aurophilic interactions existed along both the *b*- and *c*-axes to form two-dimensional structures. On careful observation of the crystal structures of **B5** and **B7**, we found that they crystallized with multiple intermolecular interactions, including not only aurophilic interactions but also CH/π interactions between neighbouring molecules. Thus these results suggest that multiple intermolecular interactions play a crucial role in forming two-dimensional structures in a crystal, such as the ones observed in the complexes **B5–B8**.

Thermochemical stability

The thermochemical stability of the Au complexes was evaluated using TGA at a heating rate of 5.0 °C min^{-1} (Fig. S3†). The temperature at which 5% weight loss occurred was defined as the thermal decomposition temperature (T_{dec}). The T_{dec} values of **B*n*** were found to be in the range of 280–295 °C, as summarized in Table 1. Comparing the thermochemical stability to the previously reported **P*n***, the **B*n*** complexes are more stable as the T_{dec} of **P*n*** (n = 5–8) are lower (253–262 °C).[9b] Analysing the TGA thermogram of **P*n***, *e.g.* **P5**, the weight loss occurred in three steps.[9b] The weight loss occurring in the first step was ~7%, which corresponded to the weight fraction of chlorine. Accordingly, the thermal decomposition process in **P*n*** was initiated with the bond cleavage of Au–Cl to eliminate the chlorine atoms.[9b] For **B*n***, the TGA thermograms showed that the dissociation of the alkoxy segment occurred during the first weight-loss step (18% for **B5**). Thus, we can conclude that switching the core structure from a phenyl to a biphenyl group resulted in an alteration of the thermal decomposition mechanism and an enhancement in the thermochemical stability of the presented Au complexes.

Table 1 Phase transition behaviour and photophysical properties of Au complexes

		Phase transition behaviour[a]	T_{dec}[b] [°C]	Φ_{PL} [%]	τ[c] [μs] (amplitude [%])
B3	Heating	Cry_1 218 Sme A	280	5	3.22 (99), 17.9 (1)
	Cooling	Cry_x 190 Sme A			
B4	Heating	Cry_1 60 Cry_2 163 Cry_3 170 Sme A	286	12	1.68 (99), 14.6 (1)
	Cooling	Cry_x 46 Cry_2 157 Sme A			
B5	Heating	Cry_1 143 Sme A	293	34	14.0 (99), 73.7 (1)
	Cooling	Cry_x 130 Sme A			
B6	Heating	Cry_1 72 Cry_2 142 Sme A	290	37	26.2 (95), 123 (5)
	Cooling	Cry_x 49 Cry_3 145 Sme A			
B7	Heating	Cry_1 99 Cry_2 114 Cry_3 130 Sme A	295	60	31.3 (93), 150 (7)
	Cooling	Cry_x 89 Cry_4 119 Sme A			
B8	Heating	Cry_1 31 Cry_2 133 Sme A	290	66	24.9 (96), 137 (4)
	Cooling	Cry_x 126 Sme A			

[a] Determined using DSC at the second heating and cooling process with a scan rate of 5.0 °C min^{-1}. The Sme-to-isotropic phase transition temperature cannot be determined due to the decomposition. Abbreviations: Cry, crystalline; Sme A, smectic A phase. [b] Thermal decomposition temperature at which 5% weight loss occurs. [c] Lifetime was measured in the wavelength range between 450 nm and 600 nm.

Phase transition properties

We observed the phase transition behaviour of **B*n*** using DSC at a scanning rate of 5.0 °C min^{-1} and using POM. All the complexes exhibited a LC phase in both heating and cooling processes (Fig. S4†), and the phase sequences are listed in Table 1. From the optical texture observed using POM with and without the application of a shear stress to the material, the LC phase was correlated to a Sme A phase. We also observed using POM that the colour of the materials turned dark on heating to the T_{dec}, at which point the LC phase was still preserved. Thermal decomposition occurred before reaching the isotropic (Iso) phase; therefore, the LC–Iso phase transition temperature cannot be determined. However, it can be concluded that **B*n*** showed much better thermodynamic stability in the LC phase, with a wider temperature range than **P*n***, in which the LC–Iso phase transition temperature ranged from 157–172 °C, owing to the biphenyl core with a large aspect ratio.

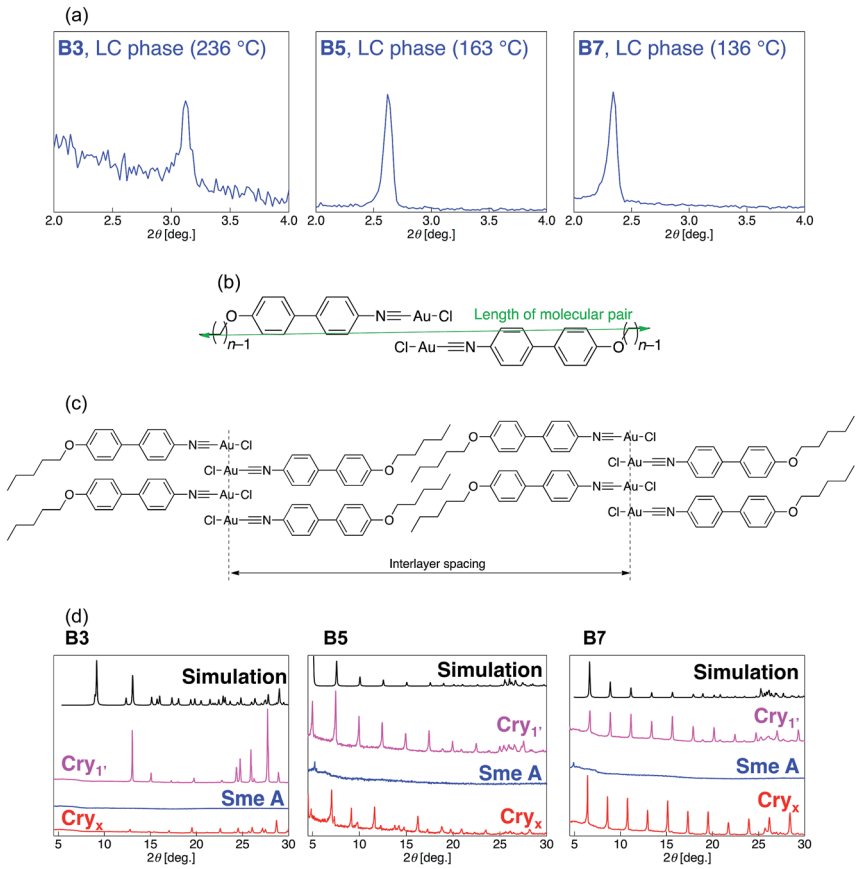

Fig. 3 (a) Small angle XRD of complexes **B3**, **B5**, and **B7** in the LC phase. (b) Molecular model of the mesogenic dimer of the complex. (c) Plausible molecular packing structure in the LC phase. (d) Wide angle XRD of the complexes in the Cry and LC phases: black, XRD pattern simulated from the single crystal X-ray analysis; pink, $Cry_{1'}$ prepared by grinding single crystals in a mortar; blue, Sme A phase; red, Cry_x frozen from Sme A phase.

In order to confirm the LC phase structure, small angle XRD measurements were performed and the obtained diffraction patterns are shown in Fig. 3a, taking complexes **B3**, **B5** and **B7** as representative examples. The diffraction appeared in a small-angle region (2.0–3.5°) for all complexes. The diffraction angles (2θ) are summarized in Table 2. We previously reported that the ***Pn*** complexes form a dimer in the LC phase, and that the dimer acts as a unit mesogen.[9b] The same mesogenic model may be applied to the present complexes (Fig. 3b). In this model, a bilayer structure was formed in the Sme A phase, as shown in Fig. 3c. The results of the XRD analysis, which show a noticeably larger molecular length than that of a single Au complex, support the hypothesis that the complexes formed dimers in the Sme A phase. Therefore, it is reasonable to assume that the dimer acts as the unit mesogen. However, the interlayer spacing of the Sme A phase was slightly shorter than the length of the molecular pairs. Therefore, we can conclude that the mesogens (dimers) were packed into a layered structure, and that the alkoxy chains of the complexes partially overlapped to form a Sme A phase, as schematically illustrated in Fig. 3c.

The wide angle XRD was measured for all complexes (Fig. 3d and S6†). In **B3**, the XRD pattern observed in $Cry_{1'}$, prepared by grinding the single crystals in a mortar, was rather different from that simulated from the crystal structure. This phenomenon was observed in the complexes with short alkoxy chains, while the same XRD pattern as the simulation was obtained from the $Cry_{1'}$ of **B5–B8**, having long alkoxy chains. Namely, the crystal structure was destroyed and changed on mechanical grinding of the complexes with short chains. As mentioned above, **B5–B8** formed well-ordered layer structures in the single crystal with multiple intermolecular interactions, while **B3** and **B4** formed dimers in the crystal structure. This structure made the molecules of **B5–B8** aggregate strongly to each other, unlike **B3–B4**. The strong aggregation with multiple interactions in **B5–B8** makes the crystal structure hard to break, and thus it did not change on mechanical grinding.

The samples from the LC phase were cooled below their freezing temperature to obtain crystals (Cry_x) and their diffraction patterns were measured. Different diffraction patterns to the initial Cry phase ($Cry_{1'}$) were observed, except for **B7**. Only **B7** showed the same diffraction pattern in both $Cry_{1'}$ and Cry_x. In **B7**, $Cry_{1'}$ showed the highest order diffraction from the well-ordered layer structure, which also appeared in Cry_x, meaning that the layer structure was successfully reconstructed in the crystal obtained after cooling from the molten state. On the other

Table 2 Interlayer spacing of the LC phase and length of mesogenic dimer estimated from single-crystal structure analysis

	2θ [°]	Interlayer spacing [Å]	Length of dimer [Å]
B3	3.12	28.3	33.2
B4	2.86	30.8	35.3
B5	2.62	33.6	36.6
B6	2.52	35.0	39.4
B7	2.34	37.7	41.7
B8	2.24	39.4	44.6

hand, the changes in the other **B*n*** complexes indicate that they could not reconstruct their initial crystal structures.

Photophysical properties

Due to the intriguing aggregated structure of **B*n***, our attention was directed toward their photophysical properties. UV-visible absorption and photoluminescence spectra in dilute chloroform solutions were measured (Fig. 4). The complexes in chloroform solution (3.0×10^{-5} mol L^{-1}) absorbed UV light at 313 nm, and the molar extinction coefficient at the absorption maxima was 3×10^4 L mol^{-1} cm^{-1}. This absorption band could be attributed to the π–π* transition of the ligand. All complexes were completely transparent in the visible light region, which is an important characteristic for light-emitting materials.

The photoluminescence spectra of **B*n*** were also measured in dilute solution (3.0×10^{-6} mol L^{-1}). In solution, a weak luminescence band was observed at around 370 nm when measured in air. When this solution was deoxygenated with argon bubbling, new emission bands appeared at 490 and 525 nm. These results indicate that the luminescence at 370 nm was fluorescence emitted from the S_1–S_0 electronic transition, and that at longer wavelengths (>470 nm) was phosphorescence emitted from the T_1–S_0 electronic transition.

In sharp contrast to their weak photoluminescence in solution, these complexes emitted intensive photoluminescence at around 500 nm in their

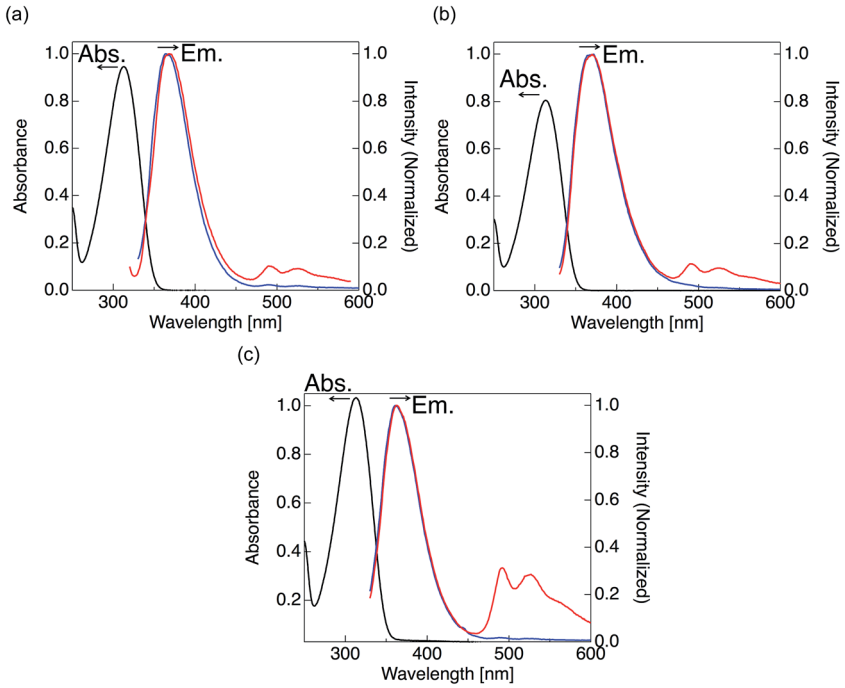

Fig. 4 Absorption (black, 3.0×10^{-5} mol L^{-1}) and corrected photoluminescence spectra (3.0×10^{-6} mol L^{-1}) in chloroform solutions of (a) **B3**, (b) **B5** and (c) **B7** ($\lambda_{ex} = 313$ nm). In the photoluminescence spectra, the red and blue lines indicate the results with and without degassed solvent, respectively.

crystal forms (Fig. 5). Strong green photoluminescence could be seen with the naked eye on UV irradiation of the crystal at 365 nm. Two luminescence bands, at 370 nm and at ~500 nm, were observed in the crystal **B3**, while crystals **B5** and **B7** showed one luminescence band at a longer wavelength. The spectral shape and wavelength of the luminescence bands were the same as those observed in dilute solution, and thus we can assign the luminescence at the shorter wavelength (370 nm) to the fluorescence and at the longer wavelength (~500 nm) to the phosphorescence.

The lifetime (τ) in the Cry phase was measured for each luminescence band separately, and the results are listed in Table 1. In the crystals **B3** and **B4**, the emission in the wavelength region of 380–450 nm decayed on the ns timescale (<4 ns), which is the same as the instrument response function of our experimental setup. In contrast, the luminescence lifetime in the wavelength range of 450–600 nm was on a microsecond timescale for all the complexes. These results clearly indicate that the luminescence band at shorter wavelengths is attributable to fluorescence, and that at longer wavelengths can be assigned to phosphorescence. This conclusion is consistent with the results observed in the luminescence spectra in dilute solutions (Fig. 4).

In all complexes, the τ at longer wavelengths could be fitted with a biexponential function, indicating the existence of two kinds of excited state. The shorter τ was the major contribution with an amplitude of >93%, while the longer τ component appeared with less than 7% amplitude. The shape of the emission

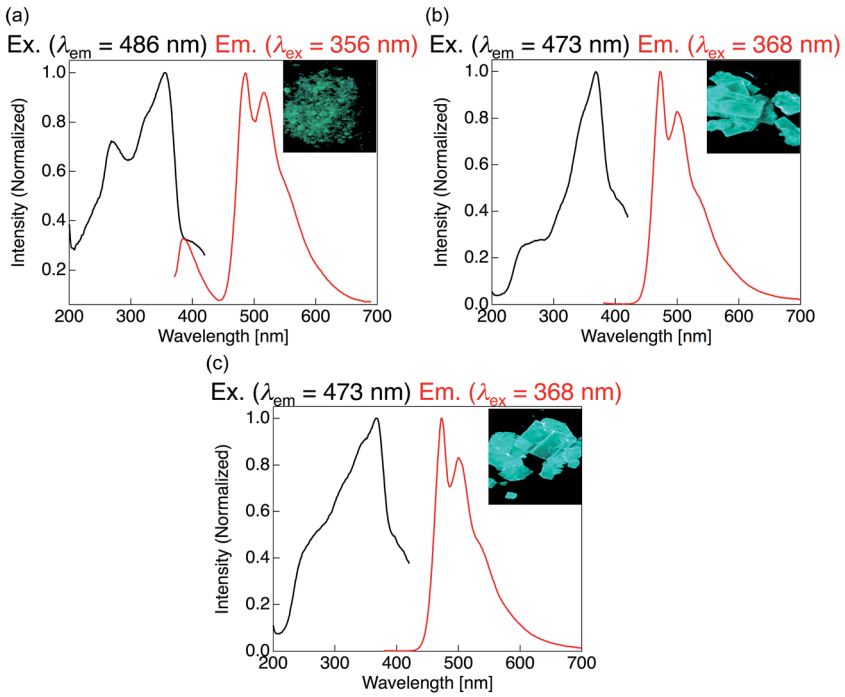

Fig. 5 Excitation (black) and corrected photoluminescence spectra (red) in the Cry_1 phase: (a), **B3**; (b), **B5**; (c), **B7**. Photographs of the crystals under UV light at 365 nm are also shown, inset.

spectra of the crystals in the wavelength region of 450–600 nm was very similar to that of the dilute solution, and thus the phosphorescence in this wavelength range indicates monomer emission. However, in the crystal form, emissions from molecular aggregates, *e.g.* excimer emission, were also observed, and are associated with the component with a longer emission lifetime.

The photoluminescence quantum yield (Φ_{PL}) of the complexes was determined for the crystal forms, and the results obtained are listed in Table 1. The Φ_{PL} for the complexes with short alkoxy chains, **B3** and **B4**, was rather small (<12%), whereas a large Φ_{PL} (>34%) was observed in the complexes with long alkoxy chains in the crystal, **B5–B8**. The difference in Φ_{PL} could be a result of the difference in the structure of the molecular aggregates, namely the crystal structure. As mentioned above, the crystal packing structure of **B3–B4** is different from that of **B5–B8**. **B3–B4** formed dimers with an aurophilic interaction, while **B5–B8** formed layer structures with multiple intermolecular interactions. This tight aggregation of **B5–B8** in the two-dimensional layer could suppress non-radiative deactivation of the excited state through vibrational and rotational motion of the molecules, resulting in a significant enhancement of the Φ_{PL} in **B5–B8** crystals.

It should be noted here that the present complexes exhibited phosphorescence with a relatively high Φ_{PL} at room temperature in air. In general, it is difficult to observe phosphorescence from organic molecules at room temperature because the rate of the radiative transition from the triplet state is much slower than that of the non-radiative pathway due to the spin-forbidden transition. Furthermore, the triplet excitation state is easily quenched by molecular oxygen in air. Although the fluorescence was quenched *via* the concentration quenching effect, especially for **B5–B8**, only the phosphorescence was remarkably enhanced on aggregation. The high Φ_{PL} for phosphorescence in the crystals of the presented Au complexes is the same phenomena reported by Tang *et al.*, *i.e.* crystallization-induced phosphorescence,[12] and this is a favourable feature for their use as practical materials.

The photoluminescence properties of the Au complexes were observed in the LC phase (Fig. 6). The luminescence intensity decreased in the Sme A phase, because at high temperatures the thermal motion of the molecules was activated, promoting the non-radiative process. The luminescence intensity was still weak in the crystals obtained on cooling the molten samples of complexes **B5**, **B6** and **B8** (Fig. 6a and S10†). On the other hand, the luminescence intensity recovered almost completely in the refrozen crystals of **B7**. The reason for this reversible change, based also on the XRD measurements, could be that the initial crystal structure was reconstructed completely only in the refrozen crystal **B7**. Therefore, the luminescence intensity could be reversibly controlled using the phase transition between the Cry and Sme A phases. The result also suggests that the photoluminescence properties are very sensitive to the structure of the molecular aggregation in the presented complexes. We have previously reported that the phase transition between the LC and Cry phases in **P*n*** altered the photoluminescence colour.[9b] However, as shown in the normalized photoluminescence spectra in Fig. 6c and d, the luminescence spectra of the **B*n*** complexes overlapped both in the Cry and LC phases, indicating that the materials show the same luminescence colour in both phases. As mentioned above, the luminescence of **B*n*** was emitted mainly by the monomer. Therefore, the luminescence colour in **B*n*** was not so sensitive to the aggregated structure of the molecules.

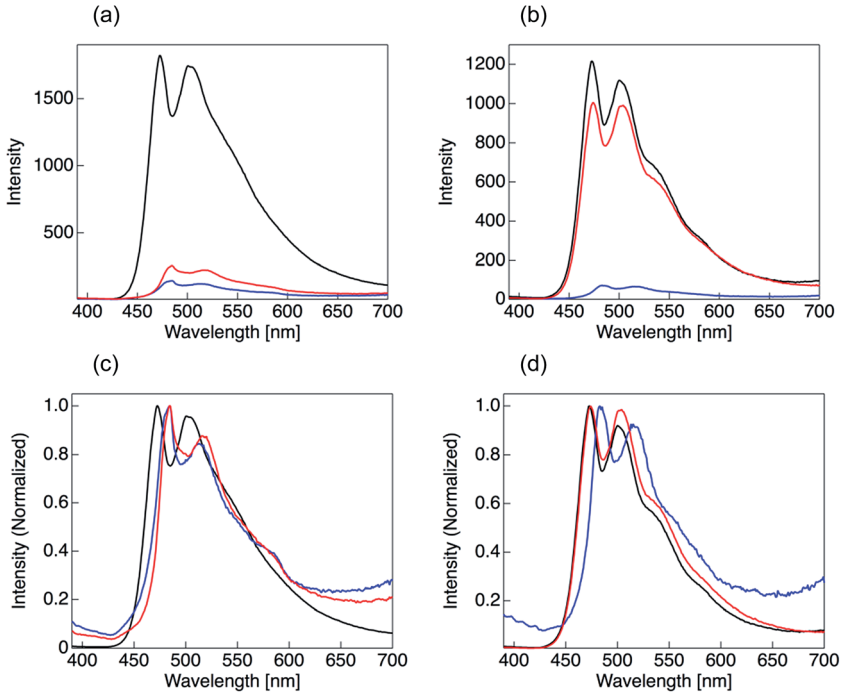

Fig. 6 Photoluminescence spectra of the complexes excited at 368 nm in the Cry_1 (black), Sme A (blue) and Cry_x phases (red): (a), **B5**; (b), **B7**, and the normalized spectra of (c), **B5**; (d), **B7**.

Conclusions

In this study, we developed new mesogenic Au complexes with a biphenyl core that can be used as AIEgens. The present Au complexes showed a higher thermochemical stability against molecular decomposition and a higher thermodynamic stability of the LC phase than in those with a phenyl core, ***Pn***, reported previously. Similar to ***Pn***, complexes **B3** and **B4** with a short alkoxy chain formed dimers in their crystal structures. However, **B5–8**, with a long alkoxy chain, formed two-dimensional structures driven by multiple intermolecular interactions in both the Cry and LC phases. All materials emitted both fluorescence and phosphorescence when in degassed dilute solutions. However, the phosphorescence was enhanced in the crystal form. Due to the tight packing of the two-dimensional structure of the crystals, molecular oxygen cannot penetrate inside the crystal, and internal vibrations and rotations of the molecules were effectively suppressed. As a consequence, the materials exhibited intensive phosphorescence with a large quantum yield (~66%) in the crystal phase. These results suggest that the mesogenic Au complexes would be useful as phosphorescent AIEgens.

Acknowledgements

The present study was supported by the MEXT-Supported Program for the Strategic Research Foundation at Private Universities, JSPS KAKENHI (15K05613), and

JST Matching Planner Program (MP27115663415). This research was also supported by the Cooperative Research Program of Network Joint Research Center for Materials and Devices (Tokyo Institute of Technology).

Notes and references

1 (*a*) W. Brütting and J. Frischeisen, in *Physics of Organic Semiconductors*, ed. W. Brütting, C. Adachi, Wiley-VCH Verlag GmbH & Co. KGaA, Weinheim, 2nd edn, 2012, ch. 15, pp. 497–539; (*b*) H. Nakanotani and C. Adachi, in *Physics of Organic Semiconductors*, ed. W. Brütting, C. Adachi, Wiley-VCH Verlag GmbH & Co. KGaA, Weinheim, 2nd edn, 2012, ch. 18, pp. 603–621.

2 (*a*) H. Sasabe and J. Kido, *J. Mater. Chem. C*, 2013, **1**, 1699–1707; (*b*) H. Sasabe and J. Kido, *Eur. J. Org. Chem.*, 2013, 7653–7663.

3 C. R. Ronda, in *Luminescence: From Theory to Applications*, ed. C. R. Ronda, Wiley-VCH Verlag GmbH & Co. KGaA, Weinheim, 2008, ch. 1, pp. 1–34.

4 J. Luo, Z. Xie, J. W. Y. Lam, L. Cheng, H. Chen, C. Qiu, H. S. Kwok, X. Zhan, Y. Liu, D. Zhu and B. Z. Tang, *Chem. Commun.*, 2001, 1740–1741.

5 (*a*) J. Mei, N. L. C. Leung, R. T. K. Kwok, J. W. Y. Lam and B. Z. Tang, *Chem. Rev.*, 2015, **115**, 11718–11940; (*b*) *Aggregation-Induced Emission: Fundamentals*, ed. A. Qin and B. Z. Tang, John Wiley & Sons, Ltd, UK, 2014; (*c*) Y. Hong, J. W. Y. Lam and B. Z. Tang, *Chem. Soc. Rev.*, 2011, **40**, 5361–5388.

6 V. W. W. Yam, V. K. M. Au and S. Y. L. Leung, *Chem. Rev.*, 2015, **115**, 7589–7728.

7 (*a*) O. Crespo, in *Modern Supramolecular Gold Chemistry*, ed. A. Laguna, Wiley-VCH Verlag GmbH & Co. KGaA, Weinheim, 2009, ch. 2, pp. 65–129; (*b*) J. M. López-de-Luzuriaga, in *Modern Supramolecular Gold Chemistry*, ed. A. Laguna, Wiley-VCH Verlag GmbH & Co. KGaA, Weinheim, 2009, ch. 6, pp. 347–401; (*c*) H. Schmidbaur and A. Schier, *Chem. Soc. Rev.*, 2012, **41**, 370–412.

8 For representative reports, see: (*a*) T. Seki, Y. Takamatsu and H. Ito, *J. Am. Chem. Soc.*, 2016, **138**, 6252–6260; (*b*) H. Ito, T. Saito, N. Oshima, N. Kitamura, S. Ishizaka, Y. Hinatsu, M. Wakeshima, M. Kato, K. Tsuge and M. Sawamura, *J. Am. Chem. Soc.*, 2008, **130**, 10044–10045; (*c*) H. Ito, M. Muromoto, S. Kurenuma, S. Ishizaka, N. Kitamura, H. Sato and T. Seki, *Nat. Commun.*, 2013, **4**, 2009, DOI: 10.1038/ncomms3009; (*d*) T. Seki, K. Sakurada, M. Muromoto and H. Ito, *Chem. Sci.*, 2015, **6**, 1491–1497.

9 (*a*) R. Kawano, O. Younis, A. Ando, Y. Rokusha, S. Yamada and O. Tsutsumi, *Chem. Lett.*, 2016, **45**, 66–68; (*b*) K. Fujisawa, Y. Okuda, Y. Izumi, A. Nagamatsu, Y. Rokusha, Y. Sadaike and O. Tsutsumi, *J. Mater. Chem. C*, 2014, **2**, 3549–3555; (*c*) K. Fujisawa, N. Kawakami, Y. Onishi, Y. Izumi, S. Tamai, N. Sugimoto and O. Tsutsumi, *J. Mater. Chem. C*, 2013, **1**, 5359–5366; (*d*) O. Yonis, Y. Rokusha, N. Sugimoto, K. Fujisawa, S. Yamada and O. Tsutsumi, *Mol. Cryst. Liq. Cryst.*, 2015, **617**, 21–31; (*e*) N. Sugimoto, S. Tamai, K. Fujisawa and O. Tsutsumi, *Mol. Cryst. Liq. Cryst.*, 2014, **601**, 97–106.

10 M. Benouazzane, S. Coco, P. Espinet and J. M. Martín-Alvarez, *J. Mater. Chem.*, 1995, **5**, 441–445.

11 H. Schmidbaur, *Gold Bull.*, 2000, **33**, 3–10.

12 (*a*) W. Z. Yuan, Y. Zhang and B. Z. Tang, in *Aggregation-Induced Emission: Applications*, ed. A. Qin and B. Z. Tang, John Wiley & Sons, Ltd, UK, 2013, ch. 2, pp. 43–60; (*b*) W. Z. Yuan, X. Y. Shen, H. Zhao, J. W. Y. Lam, L. Tang,

P. Lu, C. Wang, Y. Liu, Z. Wang, Q. Zheng, J. Z. Sun, Y. Ma and B. Z. Tang, *J. Phys. Chem. C*, 2010, **114**, 6090–6099; (*c*) Y. Gong, G. Chen, Q. Peng, W. Z. Yuan, Y. Xie, S. Li, Y. Zhang and B. Z. Tang, *Adv. Mater.*, 2015, **27**, 6195–6201.